Production of syngas from ethanol CO_2 reforming on La-doped Cu/Al_2O_3: Impact of promoter loading

Cite as: AIP Conference Proceedings **2124**, 020011 (2019); https://doi.org/10.1063/1.5117071
Published Online: 24 July 2019

Mohd-Nasir Nor Shafiqah, Trinh Duy Nguyen, Lau N. Jun, et al.

Production of Syngas from Ethanol CO_2 Reforming on La-doped Cu/Al_2O_3: Impact of Promoter Loading

Mohd-Nasir Nor Shafiqah[1], Trinh Duy Nguyen[2], Lau N. Jun[1], Mahadi B. Bahari[1] Pham T. T. Phuong[3], Bawadi Abdullah[4] and Dai-Viet N. Vo[1,5*]

[1]*Faculty of Chemical & Natural Resources Engineering, University Malaysia Pahang, Lebuhraya Tun Razak, 26300 Gambang, Kuantan, Pahang, Malaysia*
[2]*Center for Advanced Materials Research, Nguyen Tat Thanh University, Ho Chi Minh City, Viet Nam*
[3]*Institute of Chemical Technology, Vietnam Academy of Science and Technology, 1 Mac Dinh Chi Str., Dist.1, Ho Chi Minh City, Viet Nam*
[4]*Chemical Engineering Department, Universiti Teknologi PETRONAS, 31750, Tronoh, Perak, Malaysia*
[5]*Centre of Excellence for Advanced Research in Fluid Flow, Universiti Malaysia Pahang, 26300 Gambang, Kuantan, Pahang, Malaysia*

[*]Corresponding author: vietvo@ump.edu.my

Abstract. Incipient wetness impregnation (IWI) method was applied to prepared 10%Cu/Al_2O_3 whereas M%La-doped 10%Cu/Al_2O_3 (Mwt%= 1%, 2%, 3%, 4% and 5%) were synthesized by employing sequential IWI technique. The prepared catalysts were evaluated from ethanol CO_2 reforming (ECR) at 1023 K and stoichiometric feed ratio. Average crystallite size of CuO particle is reduced with La-promoter addition probably caused by lanthana dilution effect that prevent agglomeration from occur within CuO particles. H_2 reduction process produce complete CuO reduction and constant signal is appear beyond 525 K suggests that the catalysts were completely reduced beyond that temperature. 3%La catalyst identified as optimal promoter loading based on reactant conversions. C_2H_5OH and CO_2 conversions were achieved on 3%La loading is 87.6% and 55.1%, respectively. Carbon was identified on catalyst surface based on X-ray diffraction (XRD) and scanning electron microscopy (SEM).

Keywords: Ethanol dry reforming; La_2O_3; Syngas; Cu/Al_2O_3 catalyst; Hydrogen

INTRODUCTION

The diminution of fossil fuels for global energy necessities largely contribute to the environmental concerns such as air pollution as well as greenhouse emissions. Carbon dioxide (CO_2) discharged into the environment as one type of greenhouse gases lead to major environmental issues. In addition, fossil fuels known to be non-renewable resources that eventually can depleted in the future. Thus, extensive studies into renewables and environmentally friendly approach are on demand.

In addition, ethanol (C_2H_5OH) is gaining a lot of interests as a replacement of fossil fuels because of its low toxicity, low cost, high availability and renewability [1-3]. Additionally, C_2H_5OH is mostly produced from fermentation of biomass such as sugarcane, corn and wheat [4]. Furthermore, syngas (mixture of H_2 + CO) is rising as potential alternatives for sources of energy because of its renewable nature and nature-friendly [5]. Moreover, syngas can be employed for the downstream production of higher chain hydrocarbons through Fisher-Tropsch synthesis [6-7] and other petrochemical industries such as methanol, dimethyl ether (DME) and methyl tert-butyl ether (MTBE) [8-9].

6th International Conference on Environment (ICENV2018)
AIP Conf. Proc. 2124, 020011-1–020011-10; https://doi.org/10.1063/1.5117071
Published by AIP Publishing. 978-0-7354-1864-6/$30.00

Syngas production in industrial scale currently involves methane (CH_4) steam reforming and partial oxidation of CH_4 [10]. CO_2 reforming of methane is one of the most ensuring methods for syngas production because it can utilize two main types of greenhouse gases which are CO_2 and CH_4. However, this approach involves CH_4 known to be non-renewable sources that its availability will be decline in the future. In addition, steam reforming process also produces CO_2 that can negatively impact our environment.

Ethanol CO_2 reforming (ECR) is a promising approach for production of syngas because of eco-friendly method that utilizing CO_2 greenhouse gas into valuable syngas as well as consumes bio-ethanol. Additionally, from Eq. (1) ECR is the reaction between ethanol (C_2H_5OH) and carbon dioxide to produce equimolar syngas which are hydrogen (H_2) and carbon monoxide (CO).

$$C_2H_5OH + CO_2 \rightarrow 3CO + 3H_2 (\Delta H^\circ_{rxn} = 296.7 \text{ kJ mol}^{-1}) \quad (1)$$

Nevertheless, the literature available about ECR is still limited. In addition, ECR usually involves Ni catalyst because several advantages which are high availability, cost-effective and ability to break the C-C bond [11]. However, Ni-based catalysts have a few setbacks such as formation of carbon and sintering that effect catalytic activity and stability. In addition, these aforementioned drawbacks of Ni catalysts can be improved by employing noble metals catalysts (Rh, Ru, Pt, Pd and Ir) that capable to resist carbon formation in contrast to transition metals [12-14]. However, the usages of noble metals catalysts are less attractive due to cost-constrain and low availability [15]. Thus, there are several approaches taken by other researchers to improve CO_2 reforming process by introduce other types of metals.

Cu-based catalysts are frequently used in steam reforming of ethanol because of its high activity and stability as well as cost-friendly [16-17]. The ECR effect from Cu/ $Ce_{0.8}Zr_{0.2}O_2$ done by Cao et al. (2017) achieved complete ethanol conversion at 973 K [18]. In addition, Cao et al. (2018) reported the performance of oxide supports of Cu metals in ECR. The results showed Cu/CeO_2-ZrO_2 achieved full ethanol conversion at 973 K with H_2/CO ratio near to theoretical one [19]. Additionally, Cu-metals catalysts have high risks to be deactivated from formation of carbon and carbon poisoning [20]. Therefore, it is important to introduce suitable promoter and support to reduce carbon deposition and prevent catalysts deactivation. The addition of La dopants previously reported in the study of steam reforming of ethanol [21] and methane CO_2 reforming [22] to prove its oxygen storage-release capability and enhancing coke gasification. In addition, La_2O_3 promoters can enhance stability and activity of catalyst metal by improving their basicity and metal support interaction.

Nevertheless, to the best of our knowledge, there is no prior research about the effect of La-promoted over Cu/Al_2O_3 for ECR. Hence, this study's objectives were to examine the physicochemical features and performance of lanthana loading on 10% Cu/Al_2O_3 for ECR at stoichiometric condition.

EXPERIMENTAL

Catalyst Preparation

Incipient wetness impregnation (IWI) method was applied to prepared 10%Cu/Al_2O_3 whereas M%La-doped 10%Cu/Al_2O_3 (Mwt%= 1%, 2%, 3%, 4% and 5%) were synthesized by employing sequential IWI technique. γ-Al_2O_3 support (Puralox TH 100/150 supplied from Sasol) was calcined in Carbolite furnace for 6 h with 5 K min^{-1} of heating rate at 1023 K. The calcined γ-Al_2O_3 was then impregnated with prior measured volume of $Cu(NO_3)_2.3H_2O$ (Sigma-Aldrich) solution. Thereafter, the mixture was stirred employing rotary evaporator (BÜCHI Rotavapor R-200) for 3 h (323 K) and subsequently dried overnight in oven (UFB-500) at 393 K. Next, the dried sample was further calcined for 5 h at 873 K (5 K min^{-1}). Meanwhile, M%La-doped 10%Cu/Al_2O_3 were synthesized using sequential IWI technique by impregnated 10%Cu/Al_2O_3 with calculated amount of $La(NO_3)_3.6H_2O$ precursor solution (supplied from Merck). Then, the mixture was properly mixed in rotary evaporator at 323 K for 3 h. The samples were placed in the over overnight and later calcined for 5 h with temperature of 873 K.

Catalyst Characterization Methods

X-ray Diffraction (XRD) is employed to scrutinize the crystal structure, crystallite size measurement and phase identification by interaction of X-rays and sample crystals. XRD was applied by employing Cu monochromatic X-ray radiation associated with wavelength, λ = 1.5418 Å on Rigaku Miniflex II method at 15 mA and 30 kV. The powder XRD patterns at 2θ = 3°–80° were recorded with a step increment of 0.02°. Subsequently, the data from X-ray diffractogram were analyzed with the aid of Match! software (Version 3.6.2).

Temperature-programmed reduction (H_2-TPR) is conducted on a Micromeritics AutoChem II-2920 chemisorption system. Quartz U-tube was used as medium for about 0.1 g catalyst situated in between the quartz wool. Then, the catalyst was exposed to heat treatment (373 K) for 30 min with 50 ml min^{-1} of He flow. In addition, this action was to remove moisture and impurities. The sample was then reduced with 10%H_2/Ar mixture flow (50 ml min^{-1}) that act as reducing agent with temperature of 373 K to 1173 K (10 K min^{-1}). Before the sample cooled down to room temperature, it was maintained at 1173 K for 30 min.

Scanning electron microscopy (SEM) measurement was employed to study the external morphology of selected spent catalysts. SEM was operated by SmartSEM software (Carl Zeiss AG - EVO® 50). Platinum plate was applied as base for the coated sample in BAL-TEC SCD 005 Sputter Coater for about 70 s to ensure the sharpness of SEM images. The acceleration voltage in this measurement was set ranging from 5 to 16 kV.

Ethanol CO_2 Reforming Reaction

ECR was performed in fixed bed reactor (stainless steel) and situated in tubular furnace at stoichiometric feed ratio at 1023 K. Catalyst was place in the middle of reactor using quartz wool. Syringe pump was employed to inject ethanol reactant into the reactor whilst CO_2 reactant and diluent gas (N_2) were monitored through mass flow controller (Alicat). The catalyst was reduced before reaction started by reducing mixture (50%H_2/N_2) for 2 h (50 ml min^{-1}) at 973 K. Thereafter, ethanol and CO_2 at stoichiometric C_2H_5OH:CO_2 feed ratio of 1:1 was passed through the reactor with 42 L g_{cat}^{-1} h^{-1} of gas hourly space velocity (GHSV). For total 8 h of reaction, the total flow rate was sustained at 70 ml min^{-1}. Then, the effluent gas product was evaluated on gas chromatograph (GC) (Agilent GC 6890).

RESULTS AND DISCUSSION

X-Ray Diffraction

Fig. 1 illustrates the XRD analyses for fresh γ-Al_2O_3, 10%Cu/Al_2O_3 and 3%La-10%Cu/Al_2O_3. The XRD pattern was analyzed using Joint Committee on Powder Diffraction Standards (JCPDS) database [23]. The peaks listed for γ-Al_2O_3 recorded at 32.67°, 37.34°, 45.65°, and 67.02° (JCPDS card No. 04-0858) [24]. In addition, for 10%Cu/Al_2O_3 and 3%La-10%Cu/Al_2O_3, CuO phases were detected at 2θ of 32.53°, 35.56°, 38.75°, 48.75°, 58.36°, 61.57°, 75.28° (JCPDS card No. 41-0254) [25-27]. Additionally, for La_2O_3 phase diffraction peak located at 2θ = 29.87° and 53.42° (JCPDS card No. 83-1355) [24] was not spotted on La-promoted catalysts surface because of the high dispersed of La_2O_3 species and therefore, could be ascribed to fine-dispersion of La_2O_3 with the support.

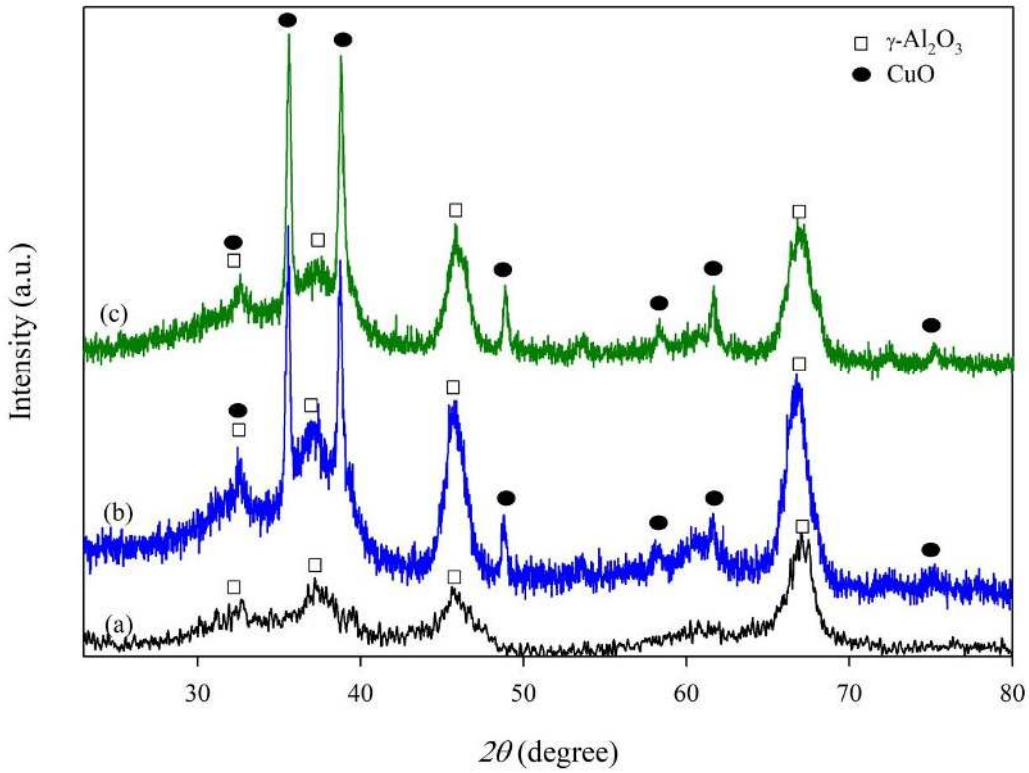

FIGURE 1. XRD analyses of fresh (a) γ-Al_2O_3, (b) 10%Cu/Al_2O_3, (c) 3%La-10%Cu/Al_2O_3.

By applying Scherrer equation [28] (see Eq. (2)), the average crystallite size, d_{CuO} of CuO particles can be calculated:

$$d_{CuO}(nm) = \frac{0.94\lambda}{\beta \cos\theta} \tag{2}$$

where, λ = X-ray wavelength, β = line broadening at half maximum intensity and θ = Bragg angle. The average crystallite size of CuO for catalysts employed in this study was summarized in the Table 1. Unpromoted 10%Cu/Al_2O_3 recorded 32.4 nm in average crystallite size with 32.4 nm while 3%La-10%Cu/Al_2O_3 recorded 27.4 nm. Moreover, the reduced in crystallite size most likely due to dilution effect of La_2O_3 that prevent agglomeration from occur within CuO particles.

TABLE 1. Summary of average crystallite size of CuO

Catalysts	**Average crystallite size of CuO, d(CuO)* (nm)**
10%Cu/Al_2O_3	32.4
3%La-10%Cu/Al_2O_3	27.4

*Average CuO crystal size was estimated using Scherrer equation for the most intense CuO peak at 2θ = 32.5°.

H_2 Temperature-programmed reduction

The reducibility of fresh catalysts was analyzed by H_2-TPR measurements shown in Fig. 2. Two peaks labelled as α and β were detected on unpromoted catalyst whereas, La-doped catalyst have one β peak. In addition, the lower temperature α peak ranging from 425 K until 470 K was assigned to the bulk-like CuO particles reduction to form Cu^0 metallic (from Eq. (3)) [29]. The peak β at higher temperature ranging from 455 K to 524 K indicated the reduction of highly dispersed CuO particles on support. Additionally, there are reports that mentioned the effect of particle size and interaction between metal-support on reduction temperature [30-31]. Furthermore, introduction of La promoter make peak α not visible due to reducing CuO crystallite size from 32.4 to 27.4 nm (Table 1). 3%La-doped catalyst has the highest reduction temperature compared to other La loadings and smallest CuO crystallite size prove that 3% loadings has the highest dispersion and Cu metal support interaction. Moreover, the signals appeared to be constant beyond 527 K suggests that the catalysts were completely reduced beyond that temperature.

$$CuO + H_2 \rightarrow Cu + H_2O \tag{3}$$

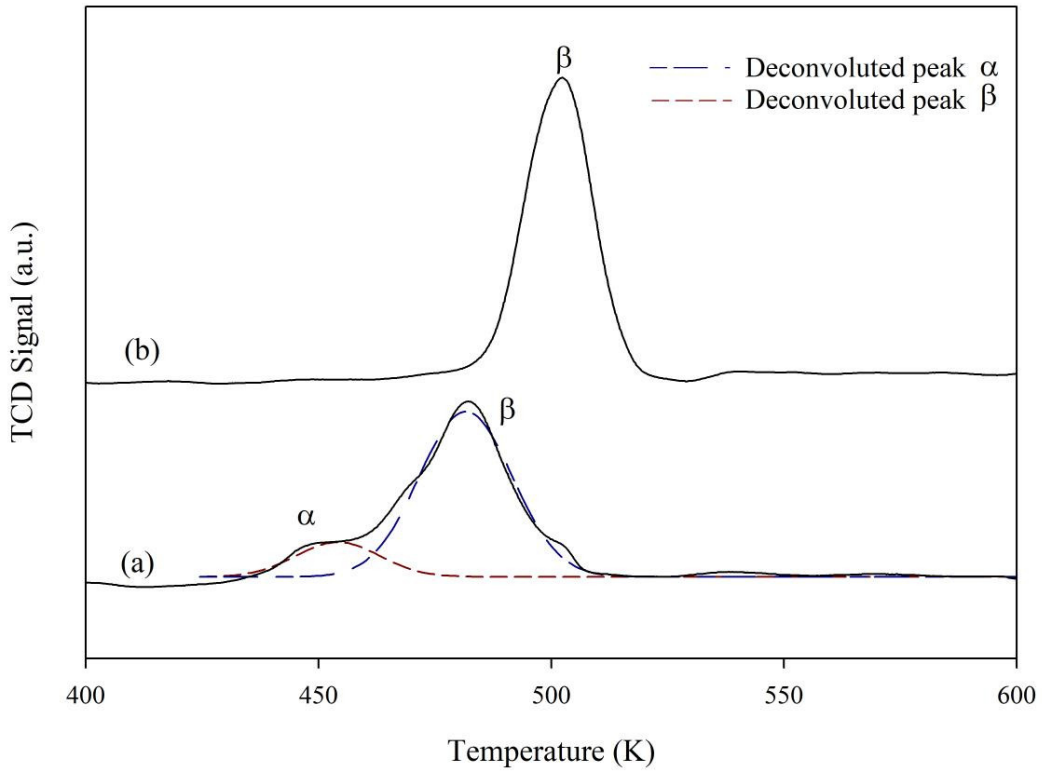

FIGURE 2. H_2-TPR of fresh (a) 10%Cu/Al_2O_3 and (b) 3%La-10%Cu/Al_2O_3.

Ethanol CO_2 Reforming Evaluation

The impact of La-promoted loading on 10%Cu/ Cu/Al_2O_3 was investigated at temperature of 1023 K stoichiometric feed ratio ($F_{CO_2} : F_{C_2H_5OH} = 1:1$). Fig. 3 illustrates the C_2H_5OH and CO_2 conversions on different promoters loading which are 10%Cu/Al_2O_3 (unpromoted), 1%La-10%Cu/Al_2O_3, 2%La-10%Cu/Al_2O_3, 3%La-10%Cu/Al_2O_3, 4%La-10%Cu/Al_2O_3 and 5%La-10%Cu/Al_2O_3. The results show that both C_2H_5OH and CO_2

conversions achieve optimal outcomes at 3%La-10%Cu/Al_2O_3. The optimal 3%La-promoted catalyst achieved 87.6% C_2H_5OH conversion and 55.1% CO_2 conversion. In addition, the improvement in both reactant conversions from incorporation of La on alumina-supported Cu-based catalyst was ascribed to La_2O_3 species redox properties that might oxidize the carbonaceous from catalysts surface and contribute in metal protection from carbon formation [32-33]. Additionally, the improvement in catalytic performance could be attributed to the basic property of lanthana that capable to enhance adsorption of CO_2 [33]. Chen et al. (2010) reported the formation of lanthanum dioxycarbonate ($La_2O_2CO_3$) from in-situ environment originated from La_2O_3 and CO_2 reaction capable to prevent formation of carbonaceous species [34].

Based on Fig. 3, reactant conversions start to drop beyond optimal 3%La loadings most likely due to limited metal dispersions in high promoter loading. Bahari et al. (2016) also reported similar trend for the effect of promoter loadings on Ni/Al_2O_3 [35].

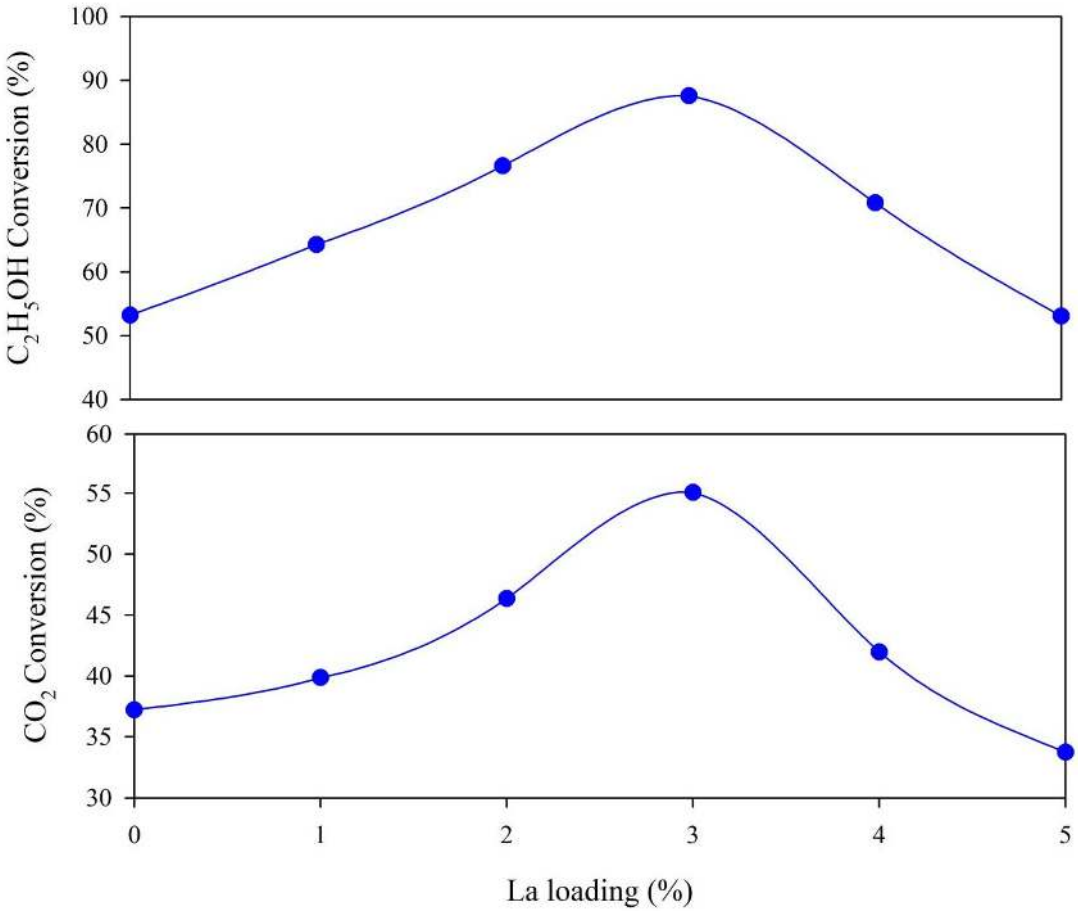

FIGURE 3. C_2H_5OH and CO_2 conversions on different promoter loadings at T=1023 K and $F_{CO_2} : F_{C_2H_5OH} = 1:1$.

CHARACTERIZATION OF SPENT CATALYSTS

X-Ray Diffraction

Fig. 4 illustrates the XRD analysis of selected catalysts after ECR at T= 1023 K and $F_{CO_2} : F_{C_2H_5OH} = 1:1$. For spent catalysts, a peak at 2θ of 26.01° was detected assigned as carbon graphite (JCPDS sheet No. 75-0444) [24]. The decomposition of C_2H_5OH and CH_4 cracking at high temperature can produce carbon species on catalyst surface [36]. In addition, high intensity new peaks were formed at 2θ = 43.3° and 51.4° and assigned as Cu metallic phase (JCPDS sheet No. 04-0836) [37] that created when undergo H_2 reduction process.

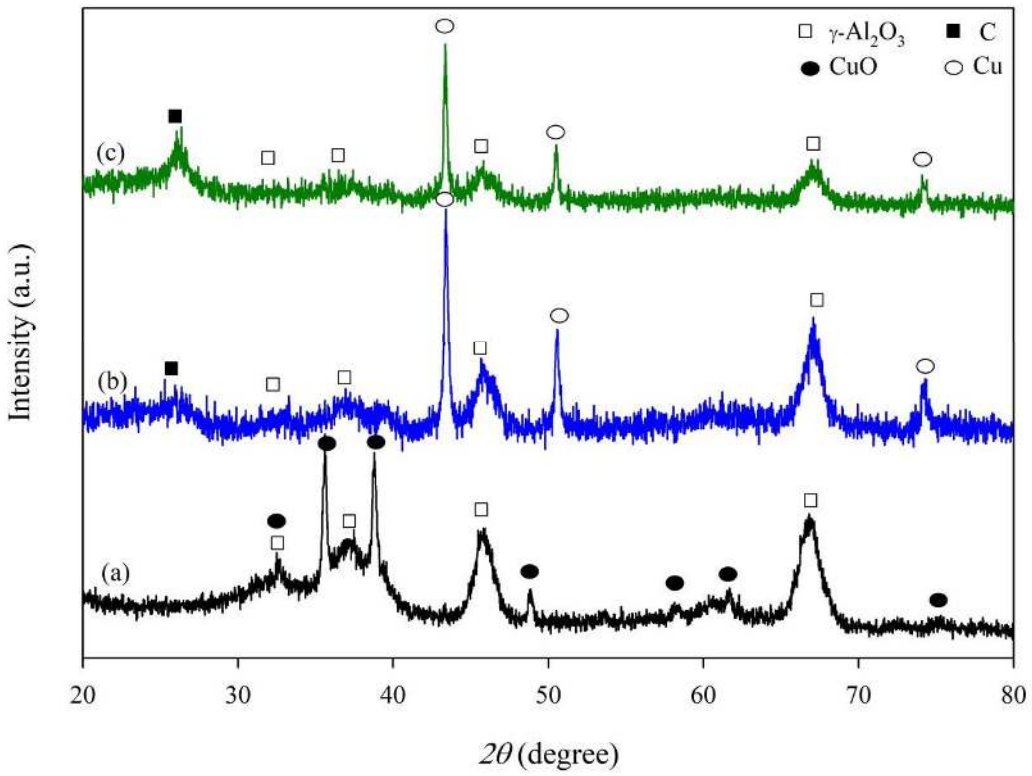

FIGURE 4. XRD analyses of (a) fresh 10%Cu/Al_2O_3, (b) spent 10%Cu/Al_2O_3 and (c) spent 3%La-10%Cu/Al_2O_3 after ECR at T=1023 K and $F_{CO_2} : F_{C_2H_5OH} = 1:1$.

Scanning Electron Microscopy

SEM images of particular spent catalysts are illustrated in Fig. 5. The images illustrate the existence of carbon nanofilaments (CNFs) on spent catalyst surface similar to other previous reports [19, 21]. In addition, the formation of CNF was originated from ethylene intermediate product, which undergoes fast polymerization process [38]. The formation of CNF that existed on catalyst surface has less impact on ECR due to its reaction with CO_2 known as reverse Boudouard reaction (Eq. (4)) [39].

$$CO_2 + C \rightarrow 2CO \quad (4)$$

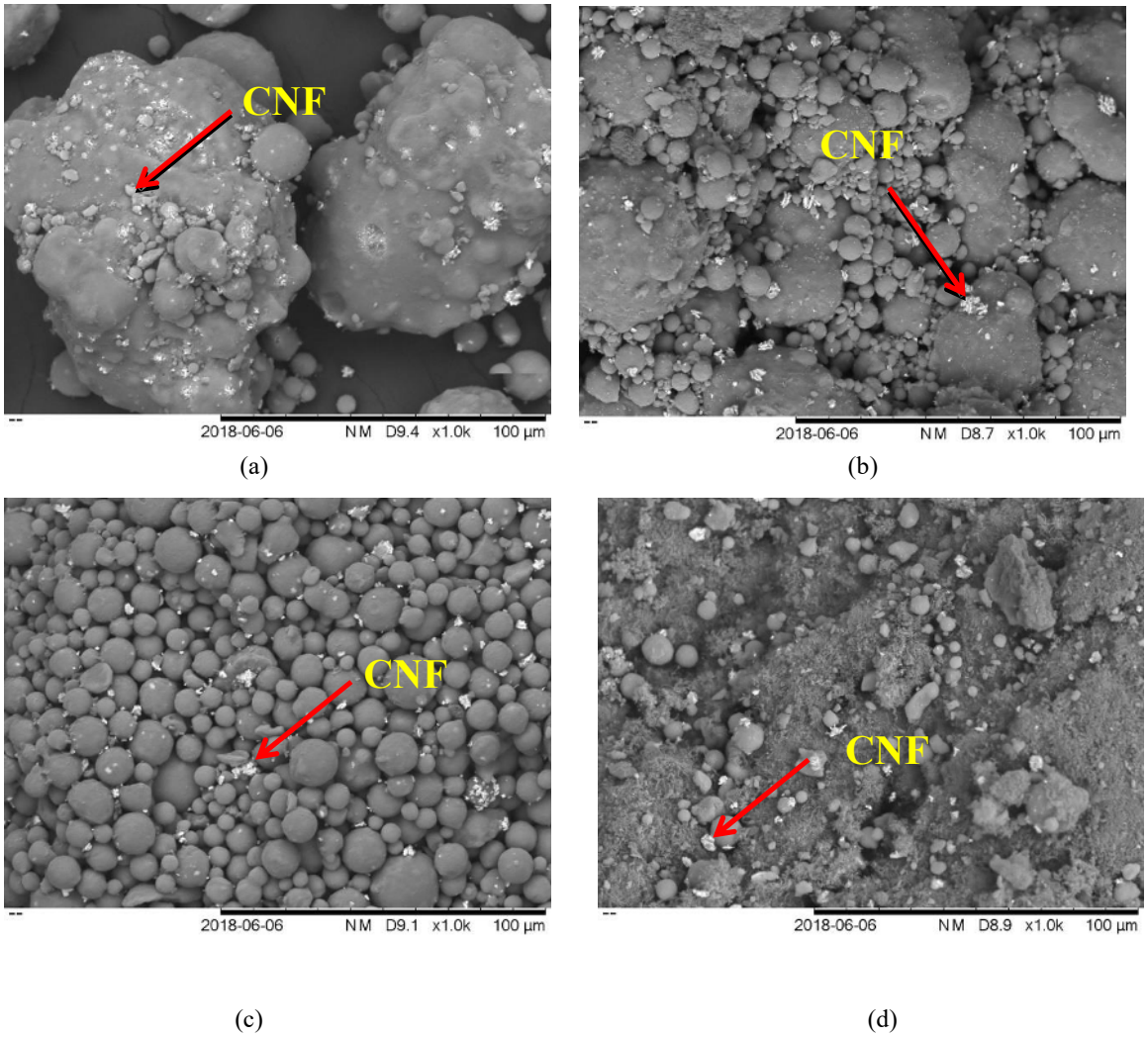

FIGURE 5. SEM analyses of spent (a) 10%Cu/Al_2O_3, (b) 2%La-10%Cu/Al_2O_3, (c) 3%La-10%Cu/Al_2O_3 and (d) 5%La-10%Cu/Al_2O_3 after ECR at T=1023 K and $F_{CO_2} : F_{C_2H_5OH} = 1:1$.

CONCLUSIONS

The IWI and sequential IWI methods were employed to synthesize 10%Cu/Al_2O_3 and promoted La catalysts, respectively. The effect of promoter loadings was investigated at T=1023 K and stoichiometric feed ratio. The interaction between Cu metal and alumina support was improved by La-doped addition by increasing reduction temperature. The catalytic performance enhanced with increasing La promoter loadings. In addition, in terms of reactant conversion, 3%La loading was selected as optimal loadings due to suppression of carbon deposition on catalyst surface. Nevertheless, beyond 3%La loadings, the catalyst performance was drop because of limited metal

dispersions in high promoter loading and caused agglomeration of Cu metal. Additionally, the highest C_2H_5OH and CO_2 conversions was 87.6% and 55.1%, respectively achieved over 3%La-10%Cu/Al_2O_3. Furthermore, XRD and SEM analyses on spent catalysts confirm the presence of carbon on catalysts surface after ECR reaction.

ACKNOWLEDGMENTS

The financial assistance from Universiti Malaysia Pahang (RDU 170326 and PGRS 180368, UMP Research Grant Scheme) is fully acknowledged by the authors. Mohd-Nasir Nor Shafiqah would like to give gratitude to Master Research Scheme (MRS) from Universiti Malaysia Pahang.

REFERENCES

1. A. Haryanto, S. Fernando, N. Murali and S. Adhikari, Energy Fuels **19**, 2098-2106 (2005).
2. L. V. Mattos, V. Jacobs, B. H. Davis and F. B. Noronha, Chem Rev **112**, 4094-4123 (2012).
3. T. Mondal, K. K. Pant, A. K. Dalai, Int J Hydrogen Energy **40**, 2529-2544 (2005).
4. V. Subramani and C. Song, R Soc Chem **20**, 65-106 (2007).
5. M. N. Barosso, M. F. Gomez, L. A. Arrúa and M. C. Abello **39**, 8712-8719 (2013).
6. B. Abdullah, N. A. Abdul Ghani and D. V. N. Vo **162**, 170-185 (2017).
7. M. Usman, W. M. A. Wan Daud and H. F. Abbas, Renew Sustain Energy Rev **45**, 710-744 (2015).
8. W. Wang S. Wang, X. Ma and J. Gong, Chem Soc Rec **40**, 3703-3727 (2011).
9. R. Yang, C. Xing, C. Lv, L. Shi and N. Tsubaki, Appl Catal A Gen **385**, 92-100 (2010).
10. L. S. Neiva and L. Gama, Braz J Petroleum Gas **4**, 119-127 (2010).
11. M. Li, X. Wang, S. Li, S. Wang and X. Ma, Int J Hydrogen Energy **35**, 6699-6708 (2010).
12. M. García-Diéguez, I. S. Pieta, M. C. Herrera, M. A. Larrubia, I. Malpartida and L. J. Alemany, Catal Today **149**, 380-387 (2010).
13. Z. Hou, P. Chen, H. Fang X. Zheng and T. Yashima, Int J Hydrogen Energy **31**, 555-561 (2006).
14. D. Zanchet, J. B. O. Santos, S. Damyanova, J. M. R. Gallo and J. M. C. Bueno, ACS Catal **5**, 3841-3863 (2015).
15. N. A. K. Aramouni, J. G. Touma, B. A Tarboush and J. Zeaiter, Renew Sustain Energy Rev **82**, 2570-2585 (2018).
16. B. Lorenzut, T. Montini, L. De Rogatis, P. Canton, A. Benedetti and P. Fornasiero, Appl Catal B Environ **101**, 397-408 (2011).
17. M. B. Gawande, A. Goswami, F. X. Felpin, T. Asefa, X. Huang, R. Silva, X. Zhou, R. Zboril and R. S. Varma, Chem Rev **116**, 3722-3811 (2016).
18. D. Cao, W. Cai, Y. Li, C. Li, H. Yu, S. Zhang and F. Qu, Catal Letters **147**, 2929-2939 (2017).
19. D. Cao, F. Zheng, Z. Zhao, W. Cai, Y. Li, H. Yu and S. Zhang, Fuel **219**, 406-416 (2018).
20. R. Ye, L. Lin, Q. Li, Z. Zhou, T. Wang, C. K. Russell, H. Adidharma, Z. Xu, Y. G. Yao and M. Fan, Catal Sci Tecnol **8**, 3428-3449 (2010).
21. P. Osorio-Vargas, N. A. Flores-González, R. M. Navarro, J. L. G. Fierro, C. H. Campos and P. Reyes, Catal Today **259**, 27-38 (2015).
22. S. Wang and G. Q. Lu, J Chem Technol Biotechnol **75**,589-595 (2000).
23. JCPDS Powder Diffraction File, International centre for diffraction data, PA: Swarthmore, 2000.
24. F. Fayaz, M.B. Bahari, T. L. M. Pham, C. Nguyen-Huy, H. D. Setiabudi, B. Abdullah and D. V. N. Vo, "Hydrogen-Rich Syngas Production via Ethanol Dry Reforming over Rare-earth Metal-promoted Co-based Catalysts," in *Recent Advancements in Biofuels and Bioenergy Utilization*, edited by P. Sarangi, S. Nanda and P. Mohanty (Springer, Singapore), pp. 177-204.
25. H. Yahiro, K. Nakaya, T. Yamamoto, K. Saiki and H. Yamaura, Catal Comm **7**, 228-231 (2006).
26. G. Castillo-Hernández, S. Mayén-Hernández, E. Castaño-Tostado, F. DeMoure-Flores, E. Campos-González, C. Martínez-Alonso and J. Santos-Cruz, Results Phys **9**, 745-752 (2018).
27. M. Chawla, V. Sharma and J. K. Randhawa, Electrocatalysis **8**, 27-35 (2017).
28. Z. Taherian, M. Yousefpour, M. Tajally and B. Khoshandam, Micropor Mesopor Mat **251**, 9-18 (2017).

29. Z. Wang and J. J. Spivey, Appl Catal A Gen **507**, 75-81 (2015).
30. D. Kim, B. S. Kwak, B. K. Min and M. Kang, Appl Surf Sci **332**, 736-746 (2015).
31. T. J. Siang, T. L. M. Pham, N. V. Cuong, P. T. T. Phuong, N. H. H. Phuc, Q. D. Truong and D. V. N. Vo, Micropor Mesopor Mat **262**, 122-132 (2018).
32. S. Y. Foo, C. K. Cheng, T. H. Nguyen and A. A. Adesina J. Mol. Catal. A: Chem **344**, 28-36 (2011).
33. U. Oemar, Y. Kathiraser, L. Mo, X. K. Ho and S. Kawi, Catal. Sci. Technol **6**, 1173-1186(2016).
34. H. Chen, H. Yu, F. Peng, H. Wang, J. Yang and M. Pan, J. Catal **269**, 281-290 (2010).
35. M. B. Bahari, B. C. Goo, T. L. M. Pham, T. J. Siang, H. T. Danh, N. Ainirazali, D. V. N. Vo, Procedia Eng **148**, 654-661 (2016).
36. N. A. Pechimuthu, K. K. Pant and S. C. Dhingra, Ind Eng Chem **1**, 1731-1736 (2007).
37. W. Li, G. Fan, L. Yang and F. Li, Green Chem **19**, 4353-4363 (2017).
38. T. Hou, S. Zhang, Y. Chen, D. Wang and W. Cai, Renew Sustain Energy Rev **44**, 132-148 (2015).
39. M. Usman and W. M. A. Wan Daud, RSC Adv **6**, 91603-91616 (2016).